DMD Fast Forward. Published on August 26, 2020 as DOI: 10.1124/dmd.120.000131
This article has not been copyedited and formatted. The final version may differ from this version.

Title Page: Evaluation of the disconnect between hepatocyte and microsome intrinsic clearance and *in vitro in vivo* extrapolation performance.

Beth Williamson, Stephanie Harlfinger, and Dermot F. McGinnity

Drug Metabolism and Pharmacokinetics, Research and Early Development, Oncology R&D, AstraZeneca, Cambridge, UK.

DMD Fast Forward. Published on August 26, 2020 as DOI: 10.1124/dmd.120.000131
This article has not been copyedited and formatted. The final version may differ from this version.

Running Title: Intrinsic clearance disconnect and IVIVE performance.

Corresponding author: Beth Williamson

Address: Hodgkin Building, c/o Darwin Building, Unit 310, Cambridge Science Park, Milton Road, Cambridge, CB4 0WG, UK.

Email: beth.williamson1@astrazeneca.com

Number of text pages: 40

Number of tables: 2

Number of figures: 6

Number of references: 30

Number of words in the Abstract: 224

Number of words in the Introduction: 754

Number of words in the Discussion: 1804

Abbreviations: AAFE, absolute average fold error; AFE, average fold error; BSA, bovine serum albumin; CL, clearance; CLbil, biliary clearance; CLint, intrinsic clearance; CLmet, metabolic clearance; CYP, cytochrome P450; DMPK, drug metabolism and pharmacokinetics; HBSS, Hank's balanced salt solution; HH, human hepatocytes; HLM, human liver microsomes; IVIVE, *in vitro in vivo* extrapolation; ER, efflux ratio; LC-MS/MS, liquid chromatography-mass spectrometry; NADPH, nicotinamide adenine dinucleotide phosphate; NEAA, Non-essential amino acids; PK, pharmacokinetics; Pgp, P-glycoprotein; Qh, hepatic blood flow; rCYP, recombinant CYP; $t_{1/2}$, half-life; UGT, uridine 5'-diphospho-glucuronosyltransferase; Vd, volume of distribution.

DMD Fast Forward. Published on August 26, 2020 as DOI: 10.1124/dmd.120.000131
This article has not been copyedited and formatted. The final version may differ from this version.

Abstract

The use of *in vitro in vivo* extrapolation (IVIVE) from human hepatocyte (HH) and human liver microsome (HLM) stability assays is a widely accepted predictive methodology for human metabolic clearance (CLmet). However, a systematic underprediction of CLmet from both matrices appears universally apparent, which can be corrected for via an empirical regression offset. Following physiological scaling, intrinsic clearance (CLint) for compounds metabolised via the same enzymatic pathway should be equivalent for both matrices. Compounds demonstrating significantly higher HLM CLint relative to HH CLint have been encountered, posing questions on how to predict CLmet for such compounds. Here, we determined the HLM:HH CLint ratio for 140 marketed drugs/compounds and compared this ratio as a function of physiochemical properties and drug metabolism enzyme dependence; and examined methodologies to predict CLmet from both matrices. The majority (78%) of compounds displaying a high HLM:HH CLint ratio were CYP3A substrates. Using HH CLint for CYP3A substrates, the current IVIVE regression offset approach remains an appropriate strategy to predict CLmet (% compounds over-/correctly/under-predicted 27/62/11, respectively). However, using the same approach for HLM significantly overpredicts CLmet for CYP3A substrates (% compounds over-/correctly/under-predicted 56/33/11, respectively), highlighting a different IVIVE offset is required for CYP3A substrates using HLM. This work furthers the understanding of compound properties associated with a disproportionately high HLM:HH CLint ratio and outlines a successful IVIVE approach for such compounds.

Significance Statement: Oral drug discovery programs typically strive for low clearance compounds to ensure sufficient target engagement. Human liver microsomes and isolated human hepatocytes are used to optimise and predict human hepatic metabolic clearance.

DMD Fast Forward. Published on August 26, 2020 as DOI: 10.1124/dmd.120.000131
This article has not been copyedited and formatted. The final version may differ from this version.

Following physiological scaling, intrinsic clearance for compounds of the same metabolic pathway should be equivalent between matrices. However, a disconnect in intrinsic clearance is sometimes apparent. The work described attempts to further understand this phenomenon and by achieving a mechanistic understanding, improvements in clearance predictions may be realised.

DMD Fast Forward. Published on August 26, 2020 as DOI: 10.1124/dmd.120.000131
This article has not been copyedited and formatted. The final version may differ from this version.

Introduction

For oral drug discovery programs there is typically a requirement to design and develop low clearance (CL) compounds to ensure sufficient extent and duration of target engagement. Optimisation of CL is usually one of the more significant challenges in drug discovery. With hepatic metabolic elimination remaining the predominant CL pathway for drugs (Cerny 2016), the use of *in vitro in vivo* extrapolation (IVIVE) from metabolic stability assays, is a widely accepted predictive methodology for human metabolic CL (CLmet) (Williamson et al., 2020; Bowman and Benet, 2019a; Bowman and Benet, 2019b; Riley et al., 2005). IVIVE comparisons of measured *in vivo* CL in animal species can assist with developing a cross species mechanistic understanding of compound disposition. Moreover, for candidate drugs, successful prediction of an acceptable human *in vivo* CL is important to enable testing of the pharmacological hypothesis in the clinic and thus in reducing drug attrition for pharmacokinetic (PK) reasons (Hay et al., 2014; Davies et al., 2020).

Within drug discovery, two hepatic *in vitro* matrices are primarily used for metabolic stability assays to optimise and predict CLmet: human liver microsomes (HLM) and isolated human hepatocytes (HH). HLM offer the ability for enhanced-throughput intrinsic clearance (CLint) screening at relatively low cost and therefore can be used to triage suitable compounds into more expensive hepatocyte incubations. HH are regarded as the most predictive *in vitro* system since they contain the full complement of enzymes and transporters that a compound may encounter during first pass metabolism hence, they often form the basis of IVIVE for CLmet. HLM and HH CLint, corrected for unbound fraction, can be scaled to *in vivo* CLint (mL/min/kg) using physiological parameters (Table 1). Therefore, with the reasonable assumption of similar binding in the HLM and HH incubations and assuming the same metabolic pathways in both systems, the scaled HLM:HH CLint ratio should approximate 1. Indeed, an indicator of the presence of significant additional metabolic pathways, such as

DMD Fast Forward. Published on August 26, 2020 as DOI: 10.1124/dmd.120.000131
This article has not been copyedited and formatted. The final version may differ from this version.

glucuronidation, present in HH and not HLM (using only NADPH as a co-factor), would be a scaled HLM:HH CLint ratio significantly less than 1.

The commonly accepted approach for IVIVE involves inputting the CLint from HLM and HH into a mathematical model of liver perfusion, typically the 'well stirred model' (WSM) (Rowland et al., 1973; Yang et al., 2007), to predict CLmet. However, this approach leads to a systematic underprediction of CLmet for reasons not presently understood (Riley et al., 2005; Foster et al., 2011; Bowman and Benet, 2019a). Many hypotheses to account for this underprediction have been proposed (Bowman and Benet, 2019a; Williamson et al., 2020); all of which should be considered during IVIVE for key compounds. However, none of these explanations solely satisfy the systematic nature of the CLmet underprediction. To account for this underprediction an empirical correction can be applied to the *in vitro* data from hepatocytes or microsomes. This offset can be derived using a regression approach, where the derived unbound *in vitro* and *in vivo* CLint values (mL/min/kg) form a correlation line from which future predictions of unbound *in vivo* CLint values for new compounds can be made (Riley et al., 2005; Sohlenius-Sternbeck et al., 2012). Notably, this offset appears to be relatively consistent between liver matrices, species, laboratories and is independent of compound (Bowman and Benet, 2016; Riley et al., 2005; Wood et al., 2017).

Importantly, for CYP mediated disposition which remains the most prevalent CL pathway for drug-like compounds, there appears to be an overall comparable IVIVE predictive performance between HLM and HH (Chiba et al., 2009; Bowman and Benet, 2016; Riley et al., 2005). More recently, it has been postulated that under-prediction from both matrices is increased as CL increases (Bowman and Benet, 2019a) and HLM are more accurate for predicting CL of CYP3A substrates (Bowman and Benet, 2019b).

Several reports have also noted a disconnect between HLM and HH CLint (Bowman and Benet, 2019b; Stringer et al., 2008; Foster et al., 2011) whereby a scaled HLM:HH CLint

DMD Fast Forward. Published on August 26, 2020 as DOI: 10.1124/dmd.120.000131
This article has not been copyedited and formatted. The final version may differ from this version.

ratio significantly greater than 1 has been determined for specific compounds. Considerably larger CLint values in HLM relative to HH have been observed for CYP3A substrates yet intriguingly not for substrates of other drug metabolism enzymes (Bowman and Benet, 2019b). The mechanistic basis for this phenomenon has yet to be elucidated, although it has been hypothesised that this observation could be due to the overlapping substrate specificity between CYP3A and the efflux transporter, P-glycoprotein (Pgp), that is located on the hepatocyte membrane, restricting compound access to drug metabolism enzymes in hepatocytes relative to unhindered access to the same enzymes in microsomes (Bowman and Benet, 2019b), thus resulting in disproportionately lower CLint determined in HH relative to HLM.

Recently, Lombardo *et al*., published a large dataset of compounds to investigate the relationship between physicochemical properties and human PK (Lombardo et al., 2018). This dataset was utilised to investigate factors contributing to the phenomena, which we have observed in our laboratory, of the apparent disconnect between HLM and HH CLint and the predictive performance of IVIVE between matrices for such compounds. The data and analyses presented herein provide further insight regarding the HLM:HH CLint disconnect with a significant dataset of 140 marketed drugs/compounds. By achieving a mechanistic understanding, improvements in IVIVE accuracy and CL predictions may be realised.

DMD Fast Forward. Published on August 26, 2020 as DOI: 10.1124/dmd.120.000131
This article has not been copyedited and formatted. The final version may differ from this version.

Materials and Methods

Compound selection

The Lombardo dataset (Lombardo et al., 2018) comprised 1352 compounds with measured human PK parameters and physicochemical properties. The dataset was crossed referenced with compounds available in the AstraZeneca compound bank and filtered according to the following criteria:

- Compounds with a measured human CL approaching or less than liver blood flow (Qh 20.7 mL/min/kg) were included to disregard compounds with extraordinarily high CL that may have a significant extrahepatic component to their elimination.
- Only compounds with a molecular weight (MW) 150-800 and octanol:water partition coefficient LogD at pH 7.4 (LogD) 0.5-4 were included to broadly represent the typical small molecule physicochemical property space encountered in oral drug discovery.
- HLM CLint, HH CLint, human plasma protein binding (PPB) and incubational binding (fuinc) values were determined. Compounds with limits on measured values (< and >) were subsequently excluded to avoid bias.

The resulting dataset (n=140 compounds) mainly comprised biopharmaceutics class 1 compounds, predominantly cleared by hepatic metabolism, with human CL ranging 0.1 – 20 mL/min/kg. Where required, additional data was generated including: CaCo2 permeability (Papp), CaCo2 efflux, MDCK-MDR1 efflux and CYP phenotyping (if the main route of elimination was via CYP but the contribution of each isoform unknown from literature sources). Given the reasonable assumption of consistencies in fuinc between species and matrices (Winiwarter et al., 2019), fuinc in HLM or rat hepatocytes (RH) was utilised. For LogD and fuinc, experimental values were supplemented with the use of in-house *in silico* models generated from machine learning methods. Where possible, the main hepatic

DMD Fast Forward. Published on August 26, 2020 as DOI: 10.1124/dmd.120.000131
This article has not been copyedited and formatted. The final version may differ from this version.

metabolic route of elimination was obtained from literature references or using databases including the University of Washington Drug Interaction Database (DIDB) (this information was based on or an extract from DIDB Copyright University of Washington, accessed: April 2020) (Table S1). It was assumed the clinical disposition pathway obtained from the literature reflects the main metabolic pathway in HH and HLM. Only in absence of such references, additional *in vitro* reaction phenotyping data was obtained to define the main contributing enzyme (Table S1).

For all *in vitro* assays detailed below, the experimental work was conducted at the Contract Research Organisation, Pharmaron, China.

Materials

HLM (150 donors; Lot QQY and Lot 38289) were purchased from Corning or BioIVT (Shanghai, China), respectively. HH (10 donors; Lot LYB and Lot IRK) were purchased from BioIVT. Human plasma was purchased from BioIVT (mixed donors, with a minimum of 2 males and 2 females). Recombinant human CYP enzymes were purchased from CYPEX (Shanghai, China). EDTA-K2 was purchased from Beijing Chemical Reagents Company (Beijing, China). Bovine Serum Albumin (BSA) was purchased from Beijing Xinjingke Biotechnology Co., Ltd (Beijing, China). Fetal bovine serum, Hank's balanced salt solution (HBSS), Non-essential amino acids (NEAA) and the Rapid Equilibrium Device (RED) were purchased from Gibco by Thermo Fisher Scientific (Shanghai, China). Dulbecco's Modified Eagle's Medium (DMEM) was purchased from Corning. MES was purchased from Sigma (Shanghai, China). The 96-well equilibrium dialysis plate was purchased from LLC (CT, USA). All other chemicals and materials were purchased from Solarbio S&T Co., LTD (Beijing, China).

DMD Fast Forward. Published on August 26, 2020 as DOI: 10.1124/dmd.120.000131
This article has not been copyedited and formatted. The final version may differ from this version.

Determination of human hepatocyte CLint

Test compound was prepared to 10 mM in 100% DMSO and further diluted to 100 µM in 100% acetonitrile. The hepatocyte incubations were prepared in Leibovitz's L-15 Medium pH 7.4 containing 1 million hepatocytes/mL and a final compound concentration of 1 µM. Cell viability was determined using a Cellometer Vision and >80% cell viability was required to proceed with the compound incubation. The compound/cell solution (250 µL) was incubated for 2 h at 37 ^{o}C and shaken at 900 rpm on an Eppendorf Thermomixer Comfort plate shaker. Samples (20 µL) were taken at 0.5, 5, 15, 30, 45, 60, 80, 100 and 120 min and quenched with 100 µL of 100% ice cold acetonitrile. Samples were shaken at 800 rpm for 2 min and centrifuged at 4000 rpm for 20 min at 4 °C to pellet precipitated protein. The supernatant fraction was diluted 1:5 with deionised water, shaken at 1000 rpm for 2 min and further diluted 1:1 with deionised water. Samples were analysed by LC-MS/MS.

As described previously (Williamson et al., 2020), sub-micromolar K_m values (lower than compound assay concentrations) would impact CLint but occurrence is infrequent, and determination of K_m was beyond the scope of this work. Hence, 1 µM was selected as an appropriate concentration in the CLint assays.

Determination of human microsome CLint

Test compound was prepared to 10 mM in 100% DMSO and further diluted to 100 µM in 100% acetonitrile. The microsomal incubations were prepared in phosphate buffered solution pH 7.4 containing 1 mg/mL microsomal protein, 1 mM NADPH and a final compound concentration of 1 µM. Following a pre-incubation with NADPH for 8 min, reactions were initiated through the addition of the test compound (final volume 250 µL) and incubated at 37 °C in a water bath for 30 min. At each timepoint (0.5, 5, 10, 15, 20, 30 min) 20 µL of

DMD Fast Forward. Published on August 26, 2020 as DOI: 10.1124/dmd.120.000131
This article has not been copyedited and formatted. The final version may differ from this version.

incubation mixture was quenched with 100 µL of 100% ice cold acetonitrile. Samples were shaken at 800 rpm for 2 min and centrifuged at 4000 rpm for 20 min at 4 °C to pellet precipitated protein. The supernatant fraction was diluted 1:5 with deionised water, shaken at 1000 rpm for 2 min and further diluted 1:1 with deionised water. Samples were analysed by LC-MS/MS.

Determination of human plasma protein binding

Plasma protein binding was completed using a RED device. Test compound was prepared to 1 mM in 100% DMSO and further diluted in plasma to achieve a final compound concentration of 5 µM in the incubation. Immediately, 50 µL of the spiked plasma was aliquot as a control T=0 sample. The T=0 sample was matrix matched with 50 µL of blank phosphate buffer solution pH 7.4 and quenched with 400 µL of 100% ice cold acetonitrile. Phosphate buffered solution pH 7.4 (500 µL) was added to the receiver chamber of the RED device and spiked plasma (300 µL) was added to the donor chamber. The plate was covered with a gas permeable lid and incubated for 18 h at 37 °C with 5% CO_2 on an orbital shaker at 300 rpm. Remaining spiked plasma was incubated in a plastic plate for 18 h at 37 °C with 5% CO_2 on an orbital shaker at 300 rpm, representing an T=18 h sample. At the end of incubation, 50 µL of post-dialysis sample from the donor or T=18 sample and receiver wells were aliquot into separate wells and matrix matched with 50 µL of phosphate buffer solution pH 7.4 or blank plasma, respectively. The samples were subsequently quenched separately in 400 µL of ice cold 100% acetonitrile. Quenched samples, including T=0, were shaken at 1000 rpm for 10 min and centrifuged for 30 min at 4000 rpm to pellet precipitated protein. The supernatant fraction was further diluted 1:1 with deionised water for analysis by LC MS/MS. An 8 point calibration curve (1 – 7500 nM), matrix matched with plasma or phosphate buffered solution and quenched with 400 µL of ice cold 100% acetonitrile was

DMD Fast Forward. Published on August 26, 2020 as DOI: 10.1124/dmd.120.000131
This article has not been copyedited and formatted. The final version may differ from this version.

used to determine the concentration in the donor and receiver wells. Compound recovery and stability in the plasma was determined using the T=0 and T=18 samples.

Determination of fuinc

HLM or RH binding was completed using a 96-well equilibrium, dialysis plate. Test compound was prepared to 100 μM in 100% DMSO and further diluted in 1 mg/mL HLM/phosphate buffer or $1x10^6$ inactivated (1 h incubation with 1 mM 1-ABT and 1.5 mM salicylamide) RH/phosphate buffer to achieve a final compound concentration of 1 μM in the incubation. Immediately, 50 μL of the spiked RH or HLM/phosphate buffer solution was aliquot as a control T=0 sample. The T=0 sample was matrix matched with 50 μL of blank phosphate buffer solution pH 7.4 and quenched with 400 μL of 100% ice cold acetonitrile. Phosphate buffered solution pH 7.4 (150 μL) was added to the receiver chamber of the dialysis block and spiked HLM/RH suspension (150 μL) was added to the donor chamber. The plate was covered with a gas permeable lid and incubated for 4 h at 37 °C with 5% CO_2 on an orbital shaker at 350 rpm. Remaining spiked matrix was incubated in a plastic plate for 18 h at 37 °C with 5% CO_2 on an orbital shaker at 300 rpm, representing an T=18 h sample. At the end of incubation, 50 μL of post-dialysis sample from the donor or T=18 sample and receiver wells were matrix matched with 50 μL of phosphate buffer solution pH 7.4 or blank RH or HLM/phosphate buffer, respectively. The samples were subsequently quenched separately in 400 μL of ice cold 100% acetonitrile. Quenched samples were shaken at 1000 rpm for 10 min and centrifuged for 30 min at 4000 rpm to pellet precipitated protein. The supernatant fraction was further diluted 1:1 with deionised water for analysis by LC MS/MS. For RH fuinc, a 5 point calibration curve (1 – 2000 nM) was generated and for HLM fuinc a 6 point calibration curve (1–2000 nM) was generated. Each standard was matrix matched with RH or HLM/phosphate buffer and phosphate buffer solution and quenched with 400 μL

DMD Fast Forward. Published on August 26, 2020 as DOI: 10.1124/dmd.120.000131
This article has not been copyedited and formatted. The final version may differ from this version.

of ice cold 100% acetonitrile. The calibration curve was used to determine the concentration in the donor and receiver wells. Compound recovery and stability in the matrix was determined using the T=0 and T=18 samples.

Determination of CaCo2 or MDCK-MDR1 permeability and cell efflux ratio

Test compound was prepared to 10 mM in 100% DMSO and further diluted to 200 μM in 100% acetonitrile. CaCo2 and MDCK-MDR1 cells were diluted in Dulbecco's Modified Eagle's Medium (culture medium) at a density of $6.86x10^5$ and $1.56x10^6$ cells/mL, respectively. 50 μL of cell suspension was added to a 96-well transwell insert plate containing 50 μL of culture medium. The base plate contained 25 mL of culture medium. The CaCo2 cells were cultured for 14-18 days and MDCK cells were cultured for 4-8 days with culture medium replaced every other day. Once confluent (as determined by lucifer yellow) and electrical resistance was >230 ohms.cm^2 for CaCo2 or >42 ohms.cm^2 for MDCK, the cells were utilised in the assay. The cells were washed and incubated with a Hanks Balanced Salt Solution containing 25 mM HEPES, pH 7.4 (transport buffer) for 30 min. Compounds were diluted to 2 mM in 100% DMSO and then further diluted to 10 μM in transport buffer. To determine the rate of compound transport in the apical to basolateral (A-B) direction, 108 μL of the 10 μM compound solution was added to the transwell (apical) and 300 μL of transport buffer added to the receiver well (basolateral). Immediately, 8 μL from the apical compound solution was diluted in 72 μL of transport buffer and quenched with 240 μL of ice cold 100% acetonitrile; this sample represented a control T=0 sample. Similarly, to determine the rate of compound transport in the basolateral to apical (B-A) direction, 308 μL of the 10 μM compound solution was added to the receiver well (basolateral) and 100 μL of transport buffer added to the transwell (apical). A T=0 sample was immediately prepared by diluting 8 μL from the basolateral compound solution in 72 μL of transport buffer and quenching with

DMD Fast Forward. Published on August 26, 2020 as DOI: 10.1124/dmd.120.000131
This article has not been copyedited and formatted. The final version may differ from this version.

240 µL of ice cold 100% acetonitrile. The plates were then incubated at 37 ^{o}C for 2 h. At the end of the 2 h incubation, 8 µL of sample was aliquot from the donor side (apical for A-B and basolateral for B-A) and added to 72 µL of transport buffer and 240 µL of ice cold 100% acetonitrile. For the receiver compartments (basolateral for A-B and apical for B-A), 72 µL was aliquot and added to 240 µL of ice cold 100% acetonitrile. Quenched samples were shaken at 1000 rpm for 5 min and centrifuged for 20 min at 4000 rpm to pellet precipitated protein. The supernatant fraction was further diluted 1:1 with deionised water for analysis by LC MS/MS.

CYP reaction phenotyping

Test compound was prepared to 10 mM in 100% DMSO and further diluted to 200 µM in 100% acetonitrile. Recombinant human CYPs (rCYP: CYP3A4, CYP3A5, CYP2C9, CYP2C19, CYP2C8, CYP1A2, CYP2D6, CYP2E1, CYP2B6) were diluted with phosphate buffered solution pH 7.4 to achieve a final concentration of 112 pmol/mL. The diluted CYP solution was pre-incubated with test compound (final concentration 2 µM) at 37 ^{o}C for 15 min. The reaction was initiated through the addition of the 10 mM NADPH and incubated at 37 °C on a plate shaker at 100 rpm for 30 min. At each timepoint (2.5, 5, 10, 15, 20, 30 min) 30 µL of incubation mixture was quenched with 120 µL of 100% ice cold acetonitrile. Samples were shaken at 1000 rpm for 10 min and centrifuged at 4000 rpm for 20 min. The quench plate was further incubated at 4 °C for 30 min and re-centrifuged at 4000 rpm for 20 min to pellet precipitated protein. The supernatant fraction was diluted 1:1 with deionised water, shaken at 1000 rpm for 2 min and analysed by LC-MS/MS.

LC-MS/MS analysis

DMD Fast Forward. Published on August 26, 2020 as DOI: 10.1124/dmd.120.000131
This article has not been copyedited and formatted. The final version may differ from this version.

The MS/MS instrument used was either a Waters XEVO® TQ-S, Waters XEVO® TQ-D or API 4000 (AB Sciex). The ultra-mass spectrometer used for sample analysis was completed in the MRM mode (MS/MS). Reverse phase HPLC with a C18 column was used to separate the analytes. A mobile phase of 99% water/0.1% formic acid (solvent A) and a solvent phase of 99% acetonitrile/0.1% formic acid (solvent B) was used. A generic LC gradient elution was used at a flow rate of 0.5 mL/min with 95% solvent A and 5% solvent B for 0.3 min after which the concentration of solvent B was increased to 95% over 0.9 min before restoring it back to 5% for the remaining 0.5 min. Mass spectrometer methods were optimised for each compound.

For all assays, the 100% ice cold acetonitrile used to quench the samples contained internal standards to ensure efficient extraction of sample, confirm injection into the mass spectrometer and allow assessment of ionisation variability. Data was accepted if the internal standard peak area coefficient of variation was <20%.

Data analysis

The half-life ($t_{1/2}$) and subsequently the CLint of the compounds incubated in HH or HLM was calculated according to Equation 1 and 2.

$$t_{\frac{1}{2}}(min) = \frac{Ln(2)}{-slope} \quad Equation\ 1.$$

$$CL_{int}(\mu L/min/million\ cells\ or\ mg\ protein) = \frac{Ln(2) \times V}{t_{\frac{1}{2}}} \quad Equation\ 2.$$

Where, V (µL/ x10^6 cells or mg protein) is the incubation volume (µL) divided by the number of cells (x10^6) or microsomal protein content (mg) in the incubation.

The unbound fraction (fu) of the compounds in human plasma, HLM or RH was calculated according to Equation 3.

DMD Fast Forward. Published on August 26, 2020 as DOI: 10.1124/dmd.120.000131
This article has not been copyedited and formatted. The final version may differ from this version.

$$Fraction\ unbound\ (fu) = \frac{[Compound]_{Receiver}}{[Compound]_{Donor}} \quad Equation\ 3.$$

Compound recovery and stability in the relevant matrix were determined according to Equation 4 and 5.

$$Compound\ recovery\ (\%) = \frac{[Compound]_{Receiver} + [Compound]_{Donor}}{[Compound]_{T=0}} \times 100 \quad Equation\ 4.$$

$$Compound\ remaining\ at\ 18\ h\ (\%) = \frac{[Compound]_{T=18}}{[Compound]_{T=0}} \times 100 \quad Equation\ 5.$$

The $t_{1/2}$ and subsequently the CLint of the compounds incubated with rCYP was determined as detailed in Equation 6 and 7.

$$t_{\frac{1}{2}rCYP}(min) = \frac{Ln(2)}{-slope} \quad Equation\ 6.$$

$$CL_{int\ rCYP}(\mu L/min/pmol) = \frac{Ln(2) \times V}{t_{\frac{1}{2}}} \quad Equation\ 7.$$

Where, V (µL/mg protein) is the incubation volume divided by the mg of protein in the incubation.

The $CL_{int,rCYP}$ was further scaled to account for CYP450 abundance and the intersystem extrapolation factors (ISEF) utilising the respective values incorporated in Simcyp (v19) using Equation 8.

$$CL_{int,CYPi}(\mu L/min/mg\ protein) = CL_{int,rCYPi} \times CYP_i abundance \times ISEF_{CYPi} \quad Equation\ 8.$$

DMD Fast Forward. Published on August 26, 2020 as DOI: 10.1124/dmd.120.000131
This article has not been copyedited and formatted. The final version may differ from this version.

Where, CYPi is the *i*th CYP isoform tested out of *n* CYP isoforms. $CL_{int,CYPi}$ is the scaled CLint for the *i*th CYP isoform, $CL_{int,rCYPi}$ is the CLint determined for the *i*th CYP isoform in rCYP (µL/min/pmol) (Equation 7), CYPi abundance is the abundance of the *i*th CYP isoform in the HLM (pmol of P450/mg protein) and $ISEF_{CYPi}$ is the ISEF for the *i*th CYP isoform.

The scaled $CL_{int,CYP}$ values were summed to give the total scaled CLint in HLM and the contribution of each CYP isoform in HLM was determined according to Equation 9.

$$Contribution_{CYPi}(\%) = \frac{CL_{int,CYPi}}{\sum_{i=1}^{n} CL_{int,CYPi}} \times 100 \quad Equation\ 9.$$

HLM:HH CLint ratio

Scaled HH and scaled HLM CLint values (mL/min/kg, Equation 10) were compared for each compound to calculate the difference, referred to as HLM:HH CLint ratio. Specifically, scaled HLM CLint (mL/min/kg) was divided by scaled HH CLint (mL/min/kg). Assuming incubational binding was consistent between HLM and HH (Chen et al., 2017; Winiwarter et al., 2019) the difference in scaled CLint (mL/min/kg) between the matrices was expected to be ~1 (based on the physiological scaling factors noted in Table 1).

$$HLM\ or\ HH\ scaled\ CLint\ (mL/min/kg) = \left(\begin{array}{c} (microsomal\ protein\ (mg)/g\ liver \\ OR \\ hepatocellularity\ (\times 10^6)/g\ liver) \\ \\ \times \frac{liver\ weight\ (g)}{body\ weight\ (kg)} \end{array} \right) / 1000 \quad Equation\ 10.$$

IVIVE

DMD Fast Forward. Published on August 26, 2020 as DOI: 10.1124/dmd.120.000131
This article has not been copyedited and formatted. The final version may differ from this version.

To compare *in vitro* hepatic CLint and *in vivo* CL for the 140 compound set, the WSM (Equation 11) (Rowland et al., 1973; Yang et al., 2007) was applied with a regression offset to correct for the observed systematic underprediction of *in vivo* CL.

$$CLmet\ (mL/min/kg) = \frac{(Q_h \times fu \times CLint,u)}{(Q_h + fu \times CLint,u)} \quad Equation\ 11.$$

Where, CLmet is *in vivo* CL determined in plasma (assuming CL is hepatic metabolic), Qh is hepatic blood flow (mL/min/kg), fu is the free fraction determined in plasma and CLint,u is the scaled unbound intrinsic metabolic CL determined from HH or HLM (mL/min/kg).

Regression offset approach

1) HH or HLM CLint values, corrected for fuinc, were scaled to the whole liver using physiological scaling factors (Table 1, Equation 10) to generate *in vitro* CLint,u (units: mL/min/kg).

2) *In vivo* CLint (units: mL/min/kg) was back-calculated from human *in vivo* CLtotal values (*in vivo* CLint, u mL/min/kg), assuming hepatic metabolic CL, using the WSM (Equation 11) to deconvolute hepatic blood flow and fu in the blood (Yang et al., 2007).

3) Using a training set of 24 metabolically cleared drugs, the *in vitro* CLint,u and *in vivo* CLint,u values were compared for HH and HLM. A systematic underprediction of *in vivo* CLint,u from *in vitro* CLint,u was observed for both matrices. In our laboratory the regression offset required to correct the underprediction was 3-fold for HLM and HH (Riley et al., 2005; Sohlenius-Sternbeck et al., 2012).

4) For the 140 compound set, the regression offset, previously defined as 3-fold (see point 3 above), was applied prospectively to the *in vitro* CLint,u from HH and HLM and compared to the *in vivo* CLint,u values. If the CLint,u values (regression offset applied) for a compound

DMD Fast Forward. Published on August 26, 2020 as DOI: 10.1124/dmd.120.000131
This article has not been copyedited and formatted. The final version may differ from this version.

were within 3-fold of unity, CLmet was categorised as correctly predicted. Over- and under-predictions of *in vivo* CLint,u were categorised as greater than 3-fold differences.

5) For scaling without the application of a regression offset the *in vitro* CLint,u was calculated solely using the WSM (Equation 11).

CaCo2 and MDCK-MDR1 Papp (Equation 12) and subsequently efflux ratio was determined according to Equation 13.

$$Papp\ (x10^{-6}\ cm/s)\ =\ \frac{V_A}{Area \times Time} \times \frac{[Compound]_{Acceptor}}{[Compound]_{Initial\ donor}} \quad Equation\ 12.$$

Where, VA is the volume in the acceptor well, area is the surface area of the membrane and time is the total transport time.

$$Efflux\ ratio\ =\ \frac{Papp_{(B-A)}}{Papp_{(A-B)}} \quad Equation\ 13.$$

The average fold error (AFE) (Equation 14) and absolute average fold error (AAFE) (Equation 15) were calculated to determine the bias (AFE) and precision (AAFE) of the CL predictions.

$$AFE\ =\ 10^{\frac{1}{N}\Sigma\ log\left(\frac{Observed}{Predicted}\right)} \quad Equation\ 14.$$

$$AAFE\ =\ 10^{\frac{1}{N}\Sigma\left|log\left(\frac{Observed}{Predicted}\right)\right|} \quad Equation\ 15.$$

HLM:HH CLint ratio data were not normally distributed. Therefore, a Kruskal-Wallis with Dunn's multiple comparison correction was used to determine if there was a difference in

DMD Fast Forward. Published on August 26, 2020 as DOI: 10.1124/dmd.120.000131
This article has not been copyedited and formatted. The final version may differ from this version.

HLM:HH CLint ratio median between compounds for different classes e.g. ion class, main metabolising enzymes etc. To determine the Kruskal-Wallis statistic (H) and the probability (*P*) all data was pooled (ignoring the group from which the data belongs) and ranked in ascending order. The rank sums were then combined to generate the *P* value and a single statistic value termed H. A large H refers to a large difference between rank sums. If the Kruskal-Wallis test was significant a Dunn's multiple comparison was used to determine which groups were statistically different from each other by calculating a *P* value (Dinno, 2015; Weaver et al., 2017; Mcdonald, 2014a).

A paired T test was used to compare HLM and HH CLint,u for UGT, CYP1A, CYP2C, CYP2D6 and Other as the variables were normally distributed, and a Wilcoxon matched pairs signed rank test (Mcdonald, 2014b) was used to compare HLM and HH CLint,u for CYP3A as the variable was not normally distributed.

DMD Fast Forward. Published on August 26, 2020 as DOI: 10.1124/dmd.120.000131
This article has not been copyedited and formatted. The final version may differ from this version.

Results

HLM:HH CLint ratio dependencies

Assuming similar metabolic rates and routes, scaled HLM and HH CLint (*in vitro* CLint,u mL/min/kg) were expected to be equivalent (HLM:HH CLint ratio =1). In our dataset, 51% of compounds had a HLM:HH CLint ratio ~1, with a maximum observed HLM:HH CLint ratio of 15. The mean HLM:HH CLint ratio was 1.9 and the median was 1.1 for the 140 compound dataset. Inherent experimental variability in the HLM and HH *in vitro* assays was assessed (data not shown) and ~95% of replicate CLint determinations for the same compound were within 2-fold. Thus, we categorised HLM:HH CLint ratio ≥2-fold as a significant biological difference.

The HLM:HH CLint ratio was significantly different between bases (mean 2.1) and acids (mean 1.0). However, the HLM:HH CLint ratio was not significantly different between neutrals and acids or neutrals and bases (Figure 1A). HLM:HH CLint ratio was not correlated with MW, LogD, pKa, human Vd or human CL (Figure 1B-F).

The dependency between the main metabolising enzyme for compounds and HLM:HH CLint ratio was evaluated for the compound dataset. The HLM:HH CLint ratio varied between metabolising enzymes with the highest HLM:HH CLint ratio observed for CYP3A substrates (mean/median HLM:HH CLint ratio = 2.8/2.1) (Figure 2 and Table S1). The difference in *in vitro* scaled CLint between HH and HLM was significantly different for CYP3A substrates (Wilcoxon matched-pairs: P <0.0001). UGT substrates displayed a mean HLM:HH CLint ratio >1 but the median was 0.8. For CYP2C, CYP2D6 and CYP1A substrates, the HLM:HH CLint ratio was ~1 (Figure 2). The dataset also contained 16 compounds (11%, referred to as "Other" in Figure 2) that were reported to be cleared via enzymes other than the major CYPs or UGTs, or the route was not defined, the mean HLM:HH CLint ratio was 1.4. Interestingly, the vast majority (78%) of compounds with a HLM:HH CLint ratio ≥2 were CYP3A

DMD Fast Forward. Published on August 26, 2020 as DOI: 10.1124/dmd.120.000131
This article has not been copyedited and formatted. The final version may differ from this version.

substrates. CYP3A HLM:HH CLint ratio was significantly different to the ratio determined for CYP2C, CYP2D6 and 'other' substrates.

Overlapping substrate specificities between CYP3A and Pgp were investigated to understand if efflux in HH provided an explanation for the high HLM:HH CLint ratio (Figure 3). CaCo2 efflux ratio (ER) and MDCK-MDR1 ER were determined for 41 and 28 compounds, respectively, and represent compounds from all metabolising enzyme families. For compounds with an ER >2 in CaCo2 and MDCK-MDR1 cells, the mean/median HLM:HH CLint ratio was 3.8/3.1 and 2.7/2.5, respectively. This was in contrast to the compounds with an ER <2, which displayed mean/median HLM:HH CLint ratio of 1.3/1.0 and 1.6/1.1 in CaCo2 and MDCK-MDR1 cells, respectively. For compounds with a HLM:HH CLint ratio ≥2, 50% and 64% of these compounds displayed an ER >2 in Caco2 and MDCK-MDR1, respectively. For CYP3A substrates that had an HLM:HH CLint ratio ≥2, 55% had an ER >2 in Caco2 cells and 67% had an ER >2 in MDCK-MDR1 cells.

In vitro in vivo extrapolation

IVIVE accuracy of *in vivo* CLint,u was evaluated using both the regression offset approach and with no offset applied for HLM and HH as outlined in Materials and Methods. When evaluating the set of 140 compounds as a whole, IVIVE performance using the regression offset showed minimal bias and good precision for both matrices. For HH, AFE was 1.3, AAFE 2.9 and % compounds over-/correctly/under-predicted was 25/62/13, respectively, whilst for HLM AFE was 1.6, AAFE 3.6 and % compounds over-/correctly/under-predicted was 34/52/14, respectively.

Prediction accuracy using the regression offset was comparable between HLM and HH when evaluating sub-categories of UGT, CYP2D6, CYP2C, CYP1A and 'other' substrates (Figure 4 & 5). However using HLM and the regression offset approach for CYP3A substrates

DMD Fast Forward. Published on August 26, 2020 as DOI: 10.1124/dmd.120.000131
This article has not been copyedited and formatted. The final version may differ from this version.

demonstrated a clear over prediction bias (AFE 3.1, AAFE 4.8, % compounds over-/correctly/under-predicted 56/33/11, respectively) (Figure 4E, Table 2). A comparison between CYP3A and non-CYP3A substrates using HLM and the regression offset approach is shown in Figure 6. Conducting IVIVE using HLM without a regression offset for CYP3A substrates broadly corrected this over-prediction bias (AFE 1.0, AAFE 3.2, % compounds over-/correctly/under-predicted 20/61/19, respectively, Figure 6B, Table 2). However, using this approach (HLM without a regression offset) for the remaining non-CYP3A substrates led to a marked under-prediction of *in vivo* CLint,u (AFE 0.3, AAFE 4.4, % compounds over-/correctly/under-predicted 4/34/62, respectively, Figure 6B, Table 2).

Using HH and the regression offset for CYP3A substrates demonstrated no clear bias (AFE 1.6, AAFE 3.1, % compounds over-/correctly/under-predicted 27/62/11, respectively) (Figure 5E, Table 2). Likewise, a comparison between CYP3A and non-CYP3A substrates using HH showed no discernible difference in predictive performance (Figure 6C, Table 2). It followed that conducting IVIVE using HH without a regression offset resulted in a significant under-prediction bias for both CYP3A and non-CYP3A compounds (Table 2).

DMD Fast Forward. Published on August 26, 2020 as DOI: 10.1124/dmd.120.000131
This article has not been copyedited and formatted. The final version may differ from this version.

Discussion

To ensure sufficient target engagement, CL is often a key parameter to optimise before progression of oral candidate drugs into clinical development. With the majority of drugs eliminated via hepatic metabolic enzymes (Cerny 2016), low CLint in HLM and HH is targeted and the values utilised to predict human metabolic CL. A systematic underprediction of *in vivo* CLint from both these hepatic matrices appears universally apparent (Bowman and Benet, 2019a; Riley et al., 2005; Sohlenius-Sternbeck et al., 2012), although it can be corrected for via a regression offset approach (Riley et al., 2005; Sohlenius-Sternbeck et al., 2012) and has been used prospectively to allow successful prediction of *in vivo* CL for many candidate drugs in our laboratory (Davies et al., 2020).

Typically, both HLM and HH are used in drug discovery. Once scaled the HLM:HH CLint ratio should be ~1 for drugs cleared by the same drug metabolism enzyme pathways in both systems. However, significant differences between HLM and HH CLint have been highlighted by several groups (Bowman and Benet, 2019b; Stringer et al., 2008; Foster et al., 2011), and this 'HLM:HH disconnect' has also been observed in our laboratory. When encountered in drug discovery, this HLM:HH disconnect phenomena poses challenges, firstly to understand the reason(s) for differences in CLint for compounds cleared by the same enzymes and secondly to decide how to approach IVIVE for compounds that demonstrate this disconnect.

No correlation was observed between HLM:HH CLint ratio and human *in vivo* CL, human Vd, LogD, MW or compound pKa for the 140 compounds dataset (Figure 1). The lack of correlation between HLM:HH CLint ratio and pKa is consistent with the hypotheses that the pH integrity of hepatocytes in suspension is destroyed (Berezhkovskiy, 2011), resulting in the same levels of ionised species present in hepatocyte and microsome assays conducted at pH 7.4. However, there was an observation that neutrals and bases (HLM:HH CLint ratio 2.1)

DMD Fast Forward. Published on August 26, 2020 as DOI: 10.1124/dmd.120.000131
This article has not been copyedited and formatted. The final version may differ from this version.

demonstrate this HLM:HH disconnect more so than acids (HLM:HH CLint ratio 1.0) but this difference was only significant between acids and bases and would need more data, specifically using acids, to confirm. Another consideration is the potential for acids to be substrates of the hepatic organic anion transporting polypeptides (OATP) present on the membrane of HH. Active uptake into HH has the potential to become the rate limiting step for the CL of these compounds. However, as shown previously (Di et al., 2012) and further exemplified here, there was no difference in HLM:HH CLint ratio between OATP substrates (including paritaprevir, lesinurad and repaglinide (Shebley et al., 2017; DIDBa; DIDBb)) and non-OATP substrates, suggesting there is no OATP dependency for the HLM:HH CLint ratio.

Building on the work by Bowman and Benet 2019b, the association of HLM:HH CLint ratio and metabolism via the major hepatic metabolic enzymes was assessed (Figure 2). For CYP1A, CYP2C and CYP2D6 substrates, the HLM:HH CLint ratio value was ~1, consistent with the CLint routes and rates being similar between matrices. Whilst UGT substrates displayed a high mean HLM:HH CLint ratio this was influenced by 2 outliers (edaravone and mizolastine). The median HLM:HH CLint ratio was 0.8, <1, as would be expected with the additional metabolism routes present in HH *versus* HLM. In agreement with Bowman and Benet 2019b, CYP3A substrates displayed a significantly higher CLint in HLM *versus* HH. This data, conducted on such a large number of compounds confirms that this HLM:HH disconnect phenomena is highly, if not exclusively, associated by cause or effect with CYP3A substrates. This would also explain the emerging trend that acids, not typically substrates of CYP3A, tend not to demonstrate this phenomena. A thorough mechanistic understanding of the basis for the high HLM CLint relative to HH CLint and the explanation for the strong association of this phenomena towards CYP3A substrates is clearly desirable. Efflux transporter activity in hepatocytes has been hypothesised to restrict compound access

DMD Fast Forward. Published on August 26, 2020 as DOI: 10.1124/dmd.120.000131
This article has not been copyedited and formatted. The final version may differ from this version.

to metabolism enzymes in hepatocytes relative to unhindered access to the same enzymes in microsomes thus leading to a high liver microsome: hepatocyte CLint ratio (Huang et al., 2010). Hence, overlapping substrate specificities between CYP3A and Pgp (Kim et al., 1999) may contribute to the observed HLM:HH CLint disconnect (Bowman and Benet, 2019b). We considered the relationship between ER and HLM:HH CLint ratio and determined that efflux transporter substrates displayed a HLM:HH disconnect (HLM:HH CLint ratio >2) whereas non-efflux substrates demonstrated an average HLM:HH CLint ratio of ~1, the theoretical expected ratio, irrespective of the cell line used to determine efflux potential (Figure 3). These data suggest that a HLM:HH disconnect may be apparent for efflux substrates as a result of Pgp activity restricting CLint in HH relative to HLM. However, only ~50% of CYP3A substrates that displayed an HLM:HH CLint ratio ≥2 had an ER >2, as determined in either MDCK or Caco2 cells. Therefore, it would appear that the reason CYP3A substrates demonstrate this phenomenon as a class is not exclusively explained by Pgp activity. Additional confirmatory work would be beneficial to explore the dependency on HLM:HH CLint ratio with Pgp and other transporter activity. It should be noted that all efflux substrates in this dataset (where measured) were highly permeable in the CaCo2 assay suggesting passive permeability across a cell membrane was not a rate limiting factor in hepatocytes. Further, no correlation was observed between HLM:HH CLint ratio and passive permeability (data not shown). There may be further additional contributory factors than transporter activity that may lead to high HLM:HH CLint ratio. For example, whether the high HLM:HH CLint for CYP3A substrates is associated with cryopreserved and not freshly prepared HH. Hepatocyte cryopreservation would have to specifically decrease CYP3A isoform activity, possibly due to conformational changes in the enzyme or via affecting co-factor levels. Considering the high proportion of candidate drugs that are CYP3A substrates, more work in our laboratory and others is warranted.

DMD Fast Forward. Published on August 26, 2020 as DOI: 10.1124/dmd.120.000131
This article has not been copyedited and formatted. The final version may differ from this version.

Whilst the use of a regression offset approach to correct the widely reported systematic underprediction of *in vivo* CLint is a pragmatic solution to predict CL, it is not mechanistically satisfactory given the empirical nature of this approach. Similar to previous reports, from our laboratory and others (Riley et al., 2005; Sohlenius-Sternbeck et al., 2012), IVIVE predictive capability utilising the regression offset approach for the whole dataset of compounds, was broadly similar between HH and HLM; 62% and 52% of compounds predicted *in vivo* CLint,u within 3-fold from HH (AFE 1.3, AAFE 2.9) and HLM (AFE 1.6, AAFE 3.6).

Approximately 80% of compounds in this dataset with a HLM:HH CLint ratio $\geq$2 were CYP3A substrates and likewise our in-house experience with propriety AstraZeneca compounds demonstrate this phenomena being strongly associated with CYP3A substrates. Given this strong association and the preponderance of candidate drugs metabolised primarily by CYP3A, our analysis focussed on comparing and contrasting IVIVE performance for CYP3A vs non-CYP3A substrates. It was observed that using HLM with an IVIVE regression offset approach for CYP3A substrates (Figure 4E, 6A, Table 2), there was an over-prediction (>3-fold) of *in vivo* CLint,u (AFE 3.1) for 56% compounds with only 33% correctly predicted. Not using the regression offset corrected this over-prediction so that AFE approached 1 and the number of CYP3A substrates over-predicted reduced from 56% to 20% and those correctly predicted increased from 33% to 61% (Figure 6B, Table 2). This data is consistent with previous reports for CYP3A substrates which employed IVIVE without the use of a regression offset and demonstrated good IVIVE accuracy from HLM (Bowman and Benet, 2019b). However, using HLM without a regression offset for non-CYP3A substrates led to a marked under-prediction of *in vivo* CLint,u (AFE 0.3), for 62% compounds with 34% correctly predicted (Figure 6B, Table 2). This data highlights that when using HLM for IVIVE a different regression offset factor is optimal for scaling CYP3A substrates *versus*

DMD Fast Forward. Published on August 26, 2020 as DOI: 10.1124/dmd.120.000131
This article has not been copyedited and formatted. The final version may differ from this version.

non-CYP3A substrates A full mechanistic understanding is not immediately apparent but the observation of both CYP isoform and matrix dependency on IVIVE methodology to predict CLmet may help to delineate the underlying reasons in the future. Based on these analyses it is important to carefully consider IVIVE approaches so that CL is appropriately predicted from HLM data for each substrate class (Chiba et al., 2009; Bowman and Benet, 2016; Riley et al., 2005).

In contrast, for HH, no prediction bias using the IVIVE regression offset approach existed for all categories of compound, including CYP3A substrates, with 62% of such compounds correctly predicted (AFE 1.6, AAFE 3.1) (Figure 6C, Table 2). Overall using HH, IVIVE performance using the regression offset approach for the whole dataset showed minimal bias and good precision (AFE 1.3, AAFE 2.8), and correctly predicted CLint,u within 3-fold for 62% of compounds, a comparable performance to CYP3A substrates.

Further, based on the data obtained herein it is reassuring that our current approach of employing an IVIVE regression offset from data generated using HH remains a useful and applicable strategy for all compounds, irrespective of metabolism enzyme. However, in the authors' opinion, uncertainty in CLmet prediction would increase for compounds that were relatively unstable in HLM compared to a more favourable HH CLint value, which highlights the need to utilise both HLM and HH CLint data to optimise against in drug discovery. Underprediction of CL could have detrimental effects on the candidate drug progression and may even result in the termination of the clinical programme due to insufficient exposure to test the clinical hypothesis. Hence, in drug discovery, it remains an appropriate, if risk averse strategy to focus on lowering HLM in addition to HH CLint to maximise intrinsic metabolic stability. Thus the authors' recommendation remains to progress candidate drugs into the clinic with a suitable HH derived CLmet prediction and a correspondingly low HLM CLint. In addition, as a different IVIVE regression offset is now emerging for CYP3A substrates

DMD Fast Forward. Published on August 26, 2020 as DOI: 10.1124/dmd.120.000131
This article has not been copyedited and formatted. The final version may differ from this version.

using HLM, the relationship may begin to elucidate a more comprehensive mechanistic understanding of IVIVE, rather than the current empirical approach, which whilst broadly successful, can be improved upon.

In summary, this work highlights the correlation between CYP3A substrates and the HLM:HH disconnect, and the subsequent deleterious effect on the accuracy of metabolic CL predictions using HLM with our current IVIVE approach for this group of compounds. We demonstrated the HLM:HH CLint ratio is not correlated with MW, LogD, pKa, human CL or human Vd. However, more work is required to understand the association, if any, of efflux transporter activity with the HLM:HH disconnect. This work suggests a consistent IVIVE approach can be successfully applied to all compounds using HH irrespective of the main contributing metabolic enzyme and provides enhanced scaling methodologies using HLM. However, without a full mechanistic understanding of this HLM:HH disconnect phenomena, it remains our strategy to minimise both HLM as well as HH CLint.

Acknowledgements

The authors would like to acknowledge Barry Jones, Tashinga Bapiro, Simone Stahl, Michael Davies and Jolyon Faria for insightful scientific discussion throughout this work.

DMD Fast Forward. Published on August 26, 2020 as DOI: 10.1124/dmd.120.000131
This article has not been copyedited and formatted. The final version may differ from this version.

Authorship Contributions

Participated in research design: BW, SH, DM

Conducted experiments: BW

Performed data analysis: BW

Wrote or contributed to the writing of the manuscript: BW, SH, DM

DMD Fast Forward. Published on August 26, 2020 as DOI: 10.1124/dmd.120.000131
This article has not been copyedited and formatted. The final version may differ from this version.

References

Alavijeh MS, Chishty M, Qaiser MZ & Palmer AM (2005) Drug metabolism and pharmacokinetics, the blood-brain barrier, and central nervous system drug discovery. *NeuroRx* **2**: 554-71.

Berezhkovskiy LM (2011) The corrected traditional equations for calculation of hepatic clearance that account for the difference in drug ionization in extracellular and intracellular tissue water and the corresponding corrected PBPK equation. *J Pharm Sci* **100**: 1167-83.

Bowman CM & Benet LZ (2016) Hepatic Clearance Predictions from In Vitro-In Vivo Extrapolation and the Biopharmaceutics Drug Disposition Classification System. *Drug Metab Dispos* **44**: 1731-1735.

Bowman CM & Benet LZ (2019a) In Vitro-In Vivo Extrapolation and Hepatic Clearance-Dependent Underprediction. *J Pharm Sci* **108**: 2500-2504.

Bowman CM & Benet LZ (2019b) In Vitro-In Vivo Inaccuracy: The CYP3A4 Anomaly. *Drug Metab Dispos* **47**: 1368-1371.

Cerny MA (2016) Prevalence of Non-Cytochrome P450-Mediated Metabolism in Food and Drug Administration-Approved Oral and Intravenous Drugs: 2006-2015. *Drug Metab Dispos* **44**: 1246-52.

Chen S, Prieto Garcia L, Bergstrom F, Nordell P & Grime K (2017) Intrinsic Clearance Assay Incubational Binding: A Method Comparison. *Drug Metab Dispos* **45**: 342-345.

Chiba M, Ishii Y & Sugiyama Y (2009) Prediction of hepatic clearance in human from in vitro data for successful drug development. *AAPS J* **11**: 262-76.

Davies M, Jones RDO, Grime K, Jansson-Löfmark R, Fretland AJ, Winiwarter S, Morgan P & Mcginnity DF (2020) Improving the Accuracy of Predicted Human

Pharmacokinetics: Lessons Learned from the AstraZeneca Drug Pipeline Over Two Decades. *Trends in Pharmacological Sciences* **41**: 390-408.

DIDBa https://didb.druginteractionsolutions.org/drug/monograph/11166/#main-transporters

DIDBb https://didb.druginteractionsolutions.org/drug/monograph/1269/#main-transporters

Dinno A (2015) Nonparametric pairwise multiple comparisons in independent groups using Dunn's test. *The Stata Journal* **15**: 292-300.

Foster JA, Houston JB & Hallifax D (2011) Comparison of intrinsic clearances in human liver microsomes and suspended hepatocytes from the same donor livers: clearance-dependent relationship and implications for prediction of in vivo clearance. *Xenobiotica* **41**: 124-36.

Hay M, Thomas DW, Craighead JL, Economides C & Rosenthal J (2014) Clinical development success rates for investigational drugs. *Nat Biotechnol* **32**: 40-51.

Huang L, Berry L, Ganga S, Janosky B, Chen A, Roberts J, Colletti AE & Lin MH (2010) Relationship between passive permeability, efflux, and predictability of clearance from in vitro metabolic intrinsic clearance. *Drug Metab Dispos* **38**: 223-31.

Kim RB, Wandel C, Leake B, Cvetkovic M, Fromm MF, Dempsey PJ, Roden MM, Belas F, Chaudhary AK, Roden DM, Wood AJ & Wilkinson GR (1999) Interrelationship between substrates and inhibitors of human CYP3A4 and P-glycoprotein. *Pharm Res* **16**: 408-14.

Lombardo F, Berellini G & Obach RS (2018) Trend Analysis of a Database of Intravenous Pharmacokinetic Parameters in Humans for 1352 Drug Compounds. *Drug Metab Dispos* **46**: 1466-1477.

Mcdonald JH 2014a. *Handbook of Biological Statistics*, 3rd ed, p157-164, Sparky House Publishing, Baltimore, Maryland.

Mcdonald JH 2014b. *Handbook of Biological Statistics*, 3rd ed, p186-189, Sparky House Publishing, Baltimore, Maryland.

Obach RS, Lombardo F & Waters NJ (2008) Trend analysis of a database of intravenous pharmacokinetic parameters in humans for 670 drug compounds. *Drug Metab Dispos* **36**: 1385-405.

Riley RJ, Mcginnity DF & Austin RP (2005) A unified model for predicting human hepatic, metabolic clearance from in vitro intrinsic clearance data in hepatocytes and microsomes. *Drug Metab Dispos* **33**: 1304-11.

Rowland M, Benet LZ & Graham GG (1973) Clearance concepts in pharmacokinetics. *J Pharmacokinet Biopharm* **1**: 123-36.

Shebley M, Liu J, Kavetskaia O, Sydor J, De Morais SM, Fischer V, Nijsen M & Bow DaJ (2017) Mechanisms and Predictions of Drug-Drug Interactions of the Hepatitis C Virus Three Direct-Acting Antiviral Regimen: Paritaprevir/Ritonavir, Ombitasvir, and Dasabuvir. *Drug Metab Dispos* **45**: 755-764.

Sohlenius-Sternbeck AK, Jones C, Ferguson D, Middleton BJ, Projean D, Floby E, Bylund J & Afzelius L (2012) Practical use of the regression offset approach for the prediction of in vivo intrinsic clearance from hepatocytes. *Xenobiotica* **42**: 841-53.

Stringer R, Nicklin PL & Houston JB (2008) Reliability of human cryopreserved hepatocytes and liver microsomes as in vitro systems to predict metabolic clearance. *Xenobiotica* **38**: 1313-29.

Weaver KF, Morales V, Dunn SL, Godde K & Weaver PF 2017. Kruskal-Wallis. *An Introduction to Statistical Analysis in Research.*

Williamson B, Colclough N, Fretland A, Jones B, Owen R & Mcginnity D (2020) Further considerations towards an effective and efficient oncology drug discovery DMPK strategy. *Curr Drug Metab* **21**: 145-162.

Winiwarter S, Chang G, Desai P, Menzel K, Faller B, Arimoto R, Keefer C & Broccatell F (2019) Prediction of Fraction Unbound in Microsomal and Hepatocyte Incubations: A Comparison of Methods across Industry Datasets. *Mol Pharm* **16**: 4077-4085.

Wood FL, Houston JB & Hallifax D (2017) Clearance Prediction Methodology Needs Fundamental Improvement: Trends Common to Rat and Human Hepatocytes/Microsomes and Implications for Experimental Methodology. *Drug Metab Dispos* **45**: 1178-1188.

Yang J, Jamei M, Yeo KR, Rostami-Hodjegan A & Tucker GT (2007) Misuse of the well-stirred model of hepatic drug clearance. *Drug Metab Dispos* **35**: 501-2.

DMD Fast Forward. Published on August 26, 2020 as DOI: 10.1124/dmd.120.000131
This article has not been copyedited and formatted. The final version may differ from this version.

Funding Footnote

All authors are AstraZeneca employees and all work was supported by AstraZeneca.

DMD Fast Forward. Published on August 26, 2020 as DOI: 10.1124/dmd.120.000131
This article has not been copyedited and formatted. The final version may differ from this version.

Figure Legends

Figure 1. Relationship between HLM:HH CLint ratio and physicochemical properties or human PK.

Where, in A) the black box and whisker represent the median and 95% confidence intervals and the blue solid line is the mean. For all plots the solid red horizontal line represents no difference in scaled HLM and HH CLint and the dashed red horizontal lines represent a 2-fold difference in scaled HLM and HH CLint.

HLM:HH CLint ratio was significantly different between bases (mean 2.1) and acids (mean 1.0) (Kruskal-Wallis: $P < 0.0001$, H = 53.9, Dunn's: acids-bases $P = 0.036$). The HLM:HH CLint ratio was not significantly different between acids and neutrals or neutrals and bases.

Figure 2. Evaluation of HH:HLM CLint ratio and the main metabolising enzyme.

Where, the black box and whisker solid lines represent the median and 95% confidence intervals and the blue solid line is the mean. The solid red horizontal line represents no difference in scaled HLM and HH CLint and the dashed red horizontal lines represent a 2-fold difference in scaled HLM and HH CLint.

CYP3A HLM:HH CLint ratio was significantly different to CYP2C, CYP2D6 and Other (Kruskal-Wallis $P < 0.0001$, H = 29.4, Dunn's: $P = 0.0006$, $P = 0.009$ and $P = 0.03$, respectively).

Figure 3. HLM:HH CLint ratio compared to ER determined in A) Caco2 cells and B) MDCK-MDR1 cells.

Where, the solid red horizontal line represents no difference in scaled HLM and HH CLint, the dashed red horizontal lines represent a 2-fold difference in scaled HLM and HH CLint and the solid red vertical line represents the efflux transporter substrate categorisation; ≥2 =

DMD Fast Forward. Published on August 26, 2020 as DOI: 10.1124/dmd.120.000131
This article has not been copyedited and formatted. The final version may differ from this version.

efflux substrate, <2 = not an efflux substrate. Symbols represent the main metabolising enzyme: ●, UGT; ○, CYP3A; ■, CYP2D6; ▲, CYP2C; ♦, CYP1A; *, Other.

In CaCo2 the number of compounds from each metabolising enzyme group were: UGT n = 3, CYP3A n = 22, CYP2D6 n = 7, CYP2C n = 4, CYP1A n = 0, Other n = 5 and in MDCK-MDR1: UGT n = 1, CYP3A n = 16, CYP2D6 n = 5, CYP2C n = 2, CYP1A n = 2, Other n = 2.

Figure 4. IVIVE with a regression offset using HLM for substrates of drug metabolism enzyme families. A) UGT, B) CYP2C, C) CYP2D6, D) CYP1A, E) CYP3A and F) Other.

Where, the red solid line is the line of unity and the red dotted lines represent a 3-fold difference.

Figure 5. IVIVE with a regression offset using HH for substrates of drug metabolism enzyme families. A) UGT, B) CYP2C, C) CYP2D6, D) CYP1A, E) CYP3A and F) Other.

Where, the red solid line is the line of unity and the red dotted lines represent a 3-fold difference.

Figure 6. IVIVE from HLM and HH. Prediction of *in vivo* CLint,u A) using HLM with a regression offset, B) using HLM without a regression offset and C) using HH with a regression offset.

Where, the blue circles represent CYP3A substrates, large blue circles represent CYP3A substrates with a HLM:HH CLint ratio >2 and the red circles represent non-CYP3A substrates. The black solid line is the line of unity and the black dotted lines represent a 3-fold difference.

DMD Fast Forward. Published on August 26, 2020 as DOI: 10.1124/dmd.120.000131
This article has not been copyedited and formatted. The final version may differ from this version.

Table 1. Human physiological scaling factors.

Species	**Liver blood flow (Qh) (mL/min/kg)**	**Liver weight (g)**	**Body Weight (Kg)**	**Microsomal protein (mg)/g liver**	**Hepatocellularity/ g liver**
Human	20.7	1500	70	40	120×10^6

DMD Fast Forward. Published on August 26, 2020 as DOI: 10.1124/dmd.120.000131
This article has not been copyedited and formatted. The final version may differ from this version.

Table 2. IVIVE prediction accuracy with and without a regression offset for CYP3A and non-CYP3A substrates.

	Substrates	IVIVE Approach	AFE	AAFE	IVIVE Prediction (%)		
					Over	Correct	Under
HLM	CYP3A	Offset	3.1	4.8	56	33	11
		No Offset	1.1	3.2	20	61	19
	Non-CYP3A	Offset	0.9	2.8	16	68	16
		No Offset	0.3	4.4	4	34	62
HH	CYP3A	Offset	1.6	3.1	27	62	11
		No Offset	0.5	3.2	13	54	33
	Non-CYP3A	Offset	1.1	2.8	22	64	14
		No Offset	0.4	3.8	7	48	45

Figure 1

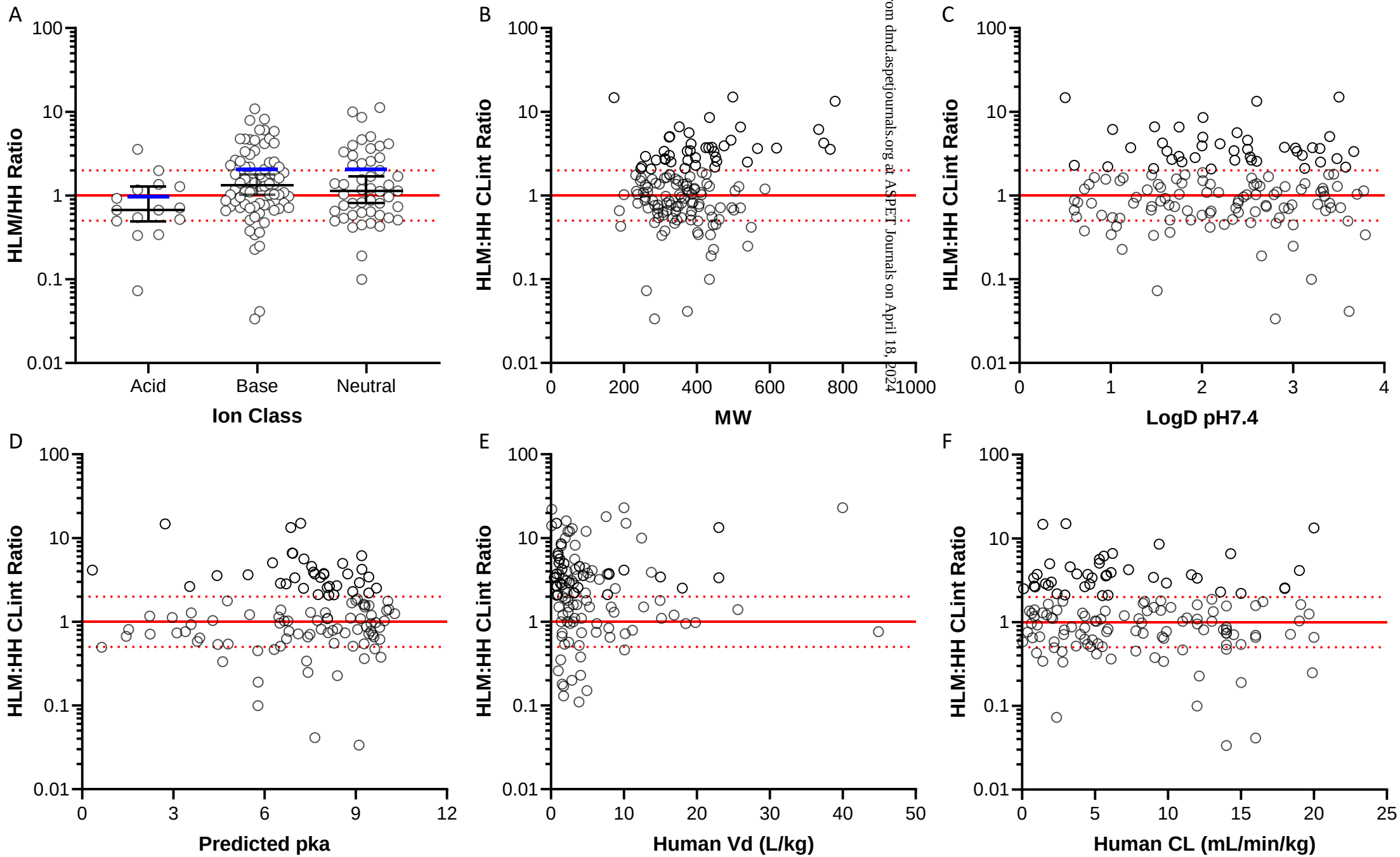

Figure 2

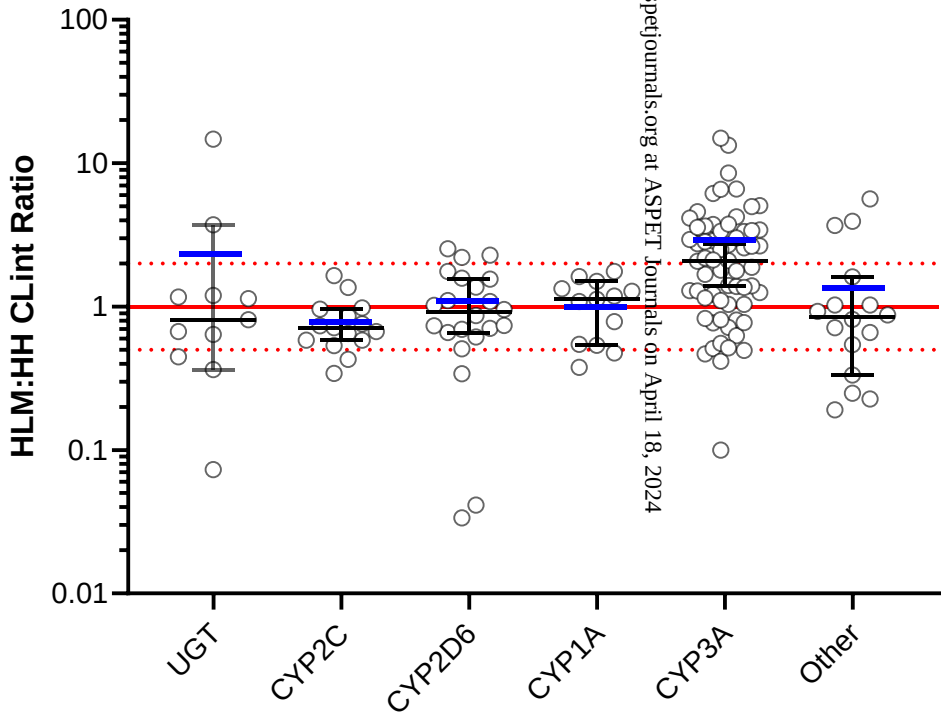

	UGT	CYP2C	CYP2D6	CYP1A	CYP3A	Other
No. of compounds	11	15	22	13	63	16
Mean	2.3	0.8	1.1	1	2.8	1.4
Median	0.8	0.7	0.9	1.1	2.1	0.9
Median 95% CI	0.4 - 3.7	0.6 - 1.0	0.7- 1.6	0.5 - 1.5	1.4 - 2.8	0.3 - 1.6

Figure 3

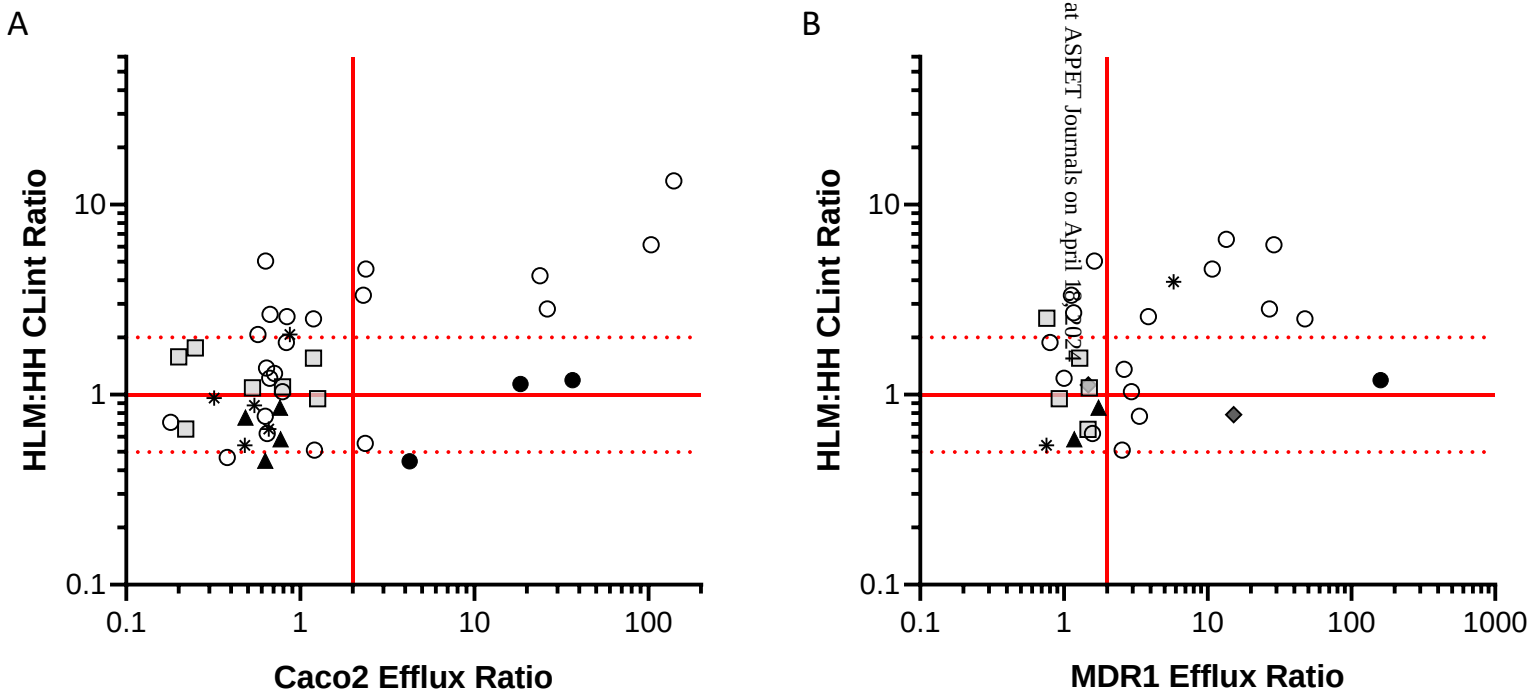

Figure 4

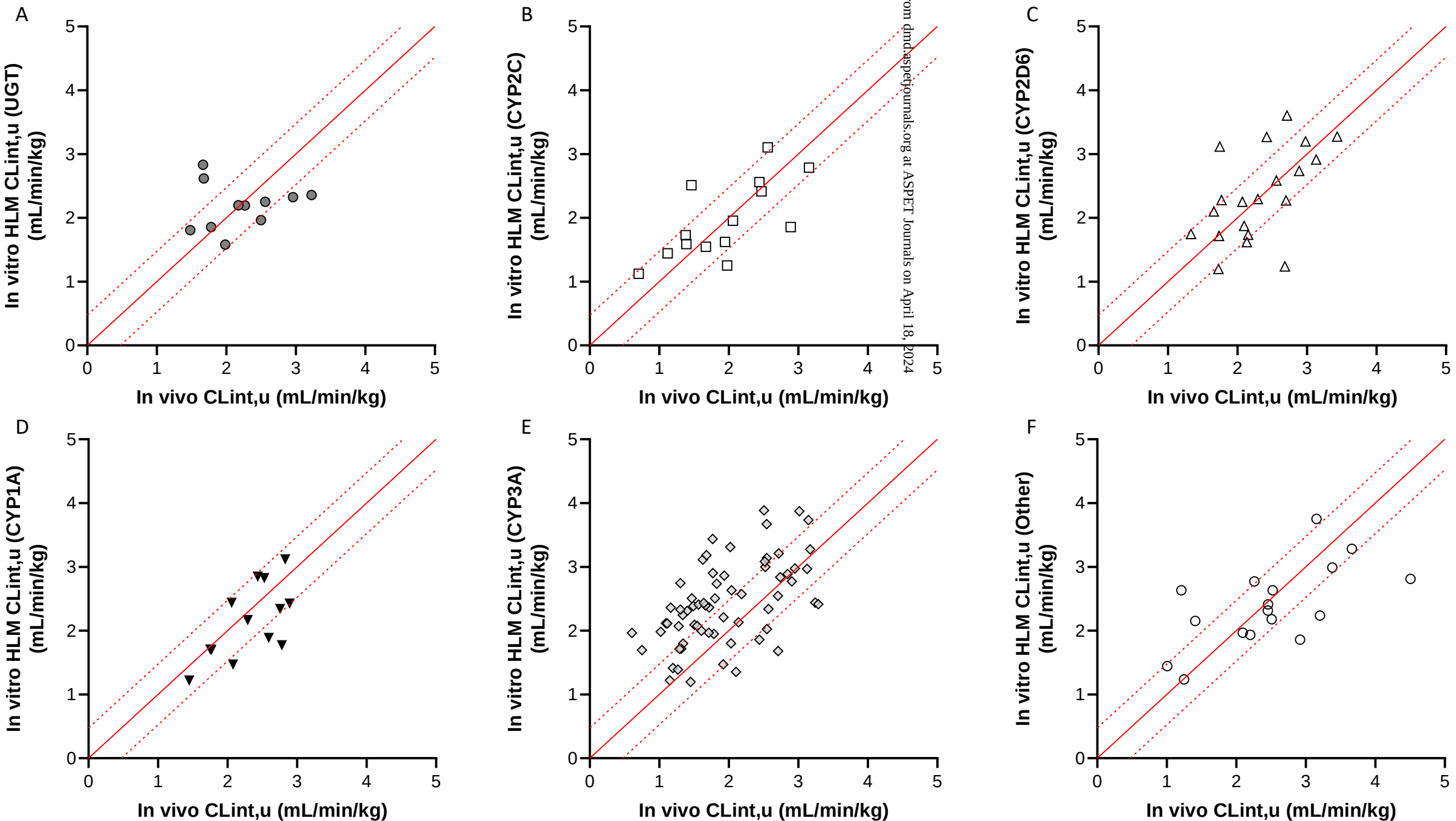

Figure 5

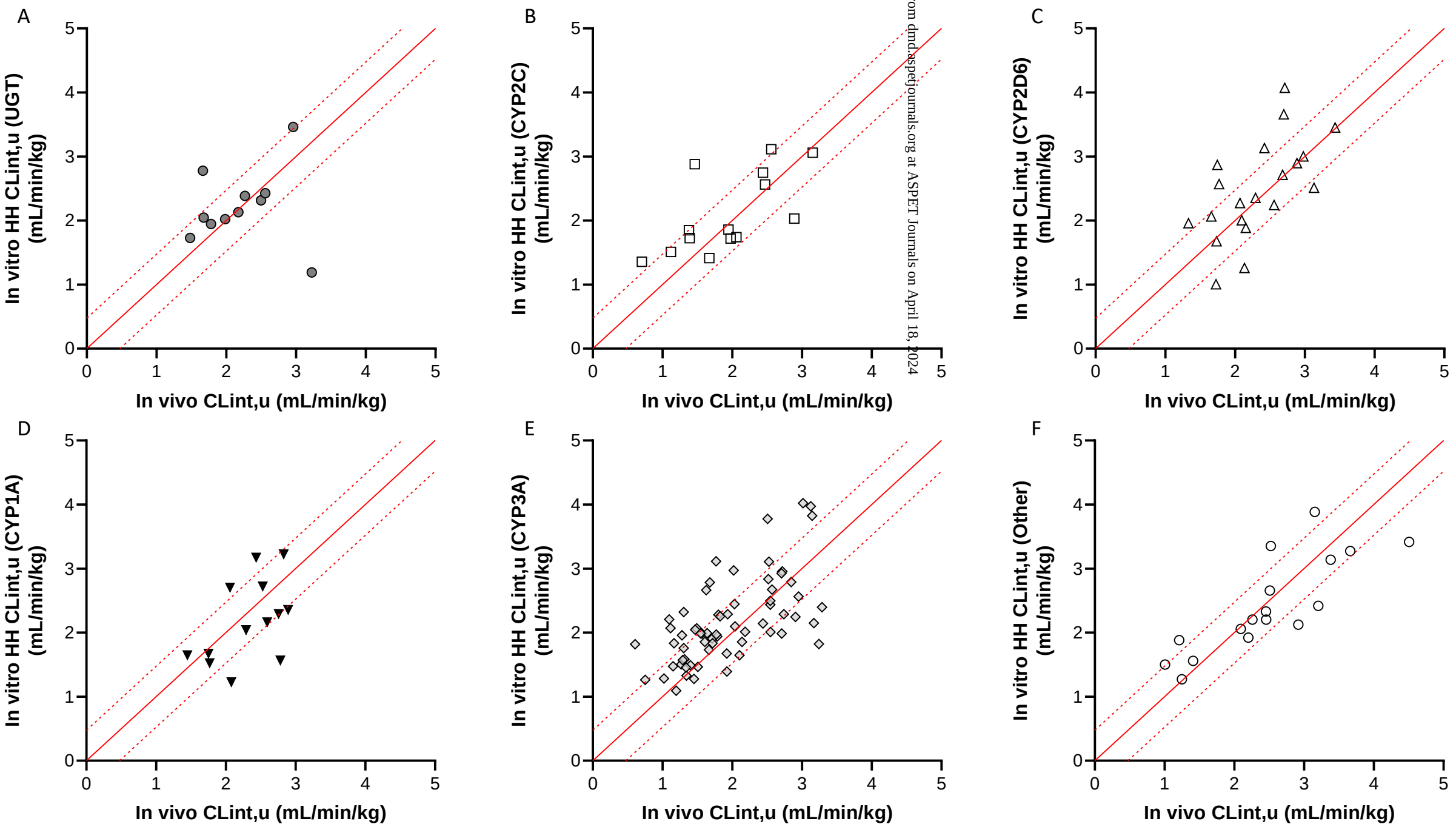

Figure 6